JMEPEG (1997) 6:219-222 

# Microstructural Characteristics of High-Temperature Oxidation in Nickel-Base Superalloy

*F.A. Khalid, N. Hussain, and K.A. Shahid*

**High-temperature oxidation behavior of a nickel-base superalloy is examined using optical and scanning electron microscopical techniques. The morphology of the oxide layers developed is examined, and EDX microanalysis reveals diffusion of the elements across the oxide-metal interface. Evidence of internal oxidation is presented, and the role of structural defects is considered. The morphology of the oxide-metal interface formed in the specimens exposed in steam and air is examined to elucidate the mechanism of high-temperature oxidation.**

**Keywords**

dendritic structure, grain and twin boundaries, interface, internal and external oxidation, oxidation, SEM linescan image, spot analysis, voids

## 1. Introduction

SUPERALLOYS are used for aerospace and nuclear applications where they can withstand high-temperature and severe oxidizing conditions. The response to high-temperature oxidation in nickel-base superalloy has been examined at different exposures in both air and steam. The alloy investigated in this study is suitable for use as tubing for reactors and other applications (Ref 1-2), and high-temperature oxidation resistance is important to achieve longer life of components.

A number of investigations on the oxidation behavior and morphology of scale formation have been documented recently (Ref 3). Various stages of oxidation in nickel alloys have been reported (Ref 4).

Previous work (Ref 5) proposed a hypothesis for the formation of voids and vacancies during formation of the oxide scale. The role of stresses developed during oxidation has been described previously (Ref 6).

In this investigation, the oxidation behavior of a nickel-base superalloy exposed to various temperatures and times in steam and air is studied. The morphology of the oxide scale formed in the specimens at different exposures and the diffusion of elements across the oxide-metal interface are examined. The nature of internal oxidation and interfacial structure is also described.

## 2. Experimental Procedure

The nominal composition of the alloy studied is given in Table 1. The alloy, known as Hastelloy C-4 (Cabot Corporation, Tuscola, IL), was received in the form of sheets, and the solution-treated specimens were cut, washed, degreased, and electrochemically polished at room temperature. Gravimetric oxidation data were generated and are described elsewhere (Ref 7). Metallographic specimens were examined in an optical and a Philips XL 30 scanning electron microscope (Philips Electronics Co., Mahwah, NJ) operated at 20 to 30 kV. Microanalysis was performed using EDX (energy dispersive x-ray) analysis.

**F.A. Khalid,** Faculty of Metallurgy and Materials Engineering, GIK Institute of Engineering Sciences and Technology, Topi, NWFP, Pakistan; and **N. Hussain** and **K.A. Shahid,** NMD, PINSTECH, PO Nilore, Islamabad, Pakistan.

## 3. Results and Discussion

### 3.1 *Microstructure and Morphology of Oxidation*

Figures 1(a) and (b) show the oxide layers formed in the specimens after exposure at 1200 °C for 6 h in steam and air, respectively. The oxide layer appeared to be compact and protective and had almost uniform thickness along the surface of the specimen exposed in steam, as compared to the cracking and spallation found in the specimen exposed in air. Figure 2 shows the external oxide layer, internal oxidation, and void formation in both metal and oxide regions in the vicinity of the oxide-metal interface. The reasons for the formation of voids and vacancies have been suggested in a previous work (Ref 5). Figure 3 reveals microstructural features after etching the specimen. Clearly, internal oxidation has formed along the grain boundaries. The round voids can also be found at the grain and twin boundaries. Internal oxidation and formation of voids can be attributed to more rapid diffusion along the grain and twin boundaries.

### 3.2 *Oxide-Metal Interface*

Figure 4 shows the interface between oxide and metal in the specimen exposed to high temperature in steam. The interface is highly irregular, and branching of arms perpendicular to the external oxide layer can be observed. The morphology of this branching appeared to be similar to a dendritic structure. Figure 5 shows another example of dendritic structure observed in the specimen exposed at 1200 °C for 400 h in steam. However, a more uniform interface between the oxide layer and the metal

**Table 1 Chemical composition of alloy**

| | Elements, wt % | | | | | | | | | | |
|---|---|---|---|---|---|---|---|---|---|---|---|
| Alloy | C | Si | Mn | Cr | Mo | Ni | Ti | Fe | Co | S | P |
| C-4 | 0.003 | 0.02 | 0.13 | 15.65 | 15.31 | 68.02 | 0.24 | 0.53 | 0.10 | 0.003 | 0.001 |

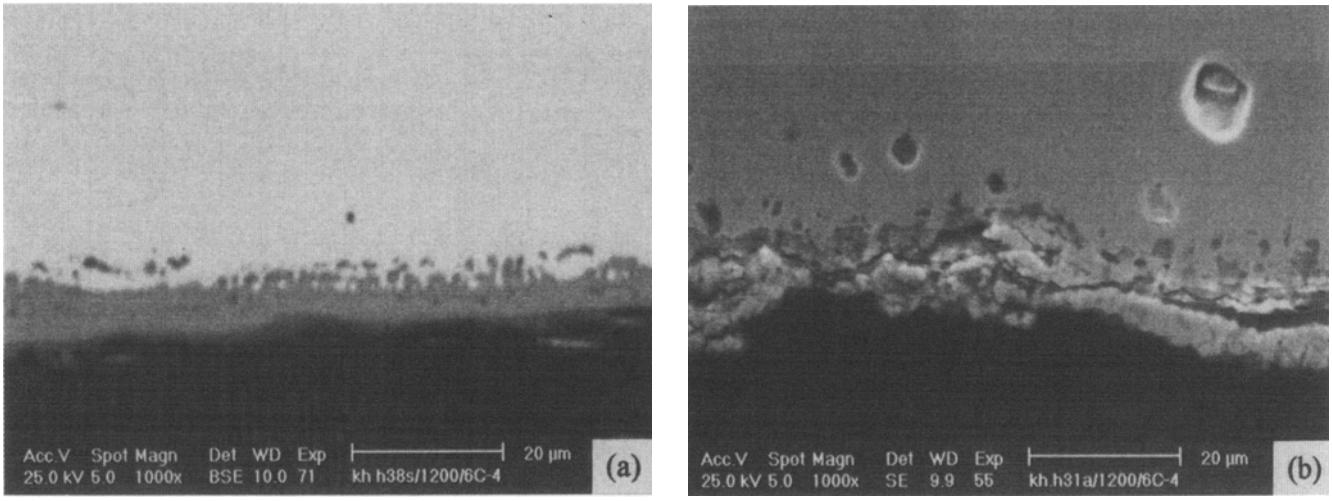


**Fig. 1** SEM micrographs showing oxide layer in the specimens exposed at 1200 °C for 6 h in (a) steam and (b) air

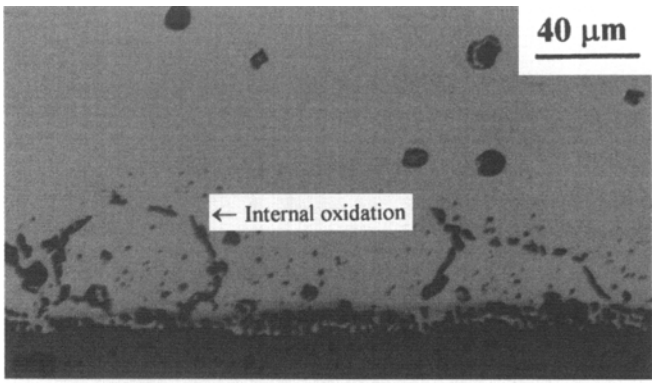


**Fig. 2** Optical micrograph showing oxide layer, internal oxidation, and voids in the specimen exposed in steam (unetched)

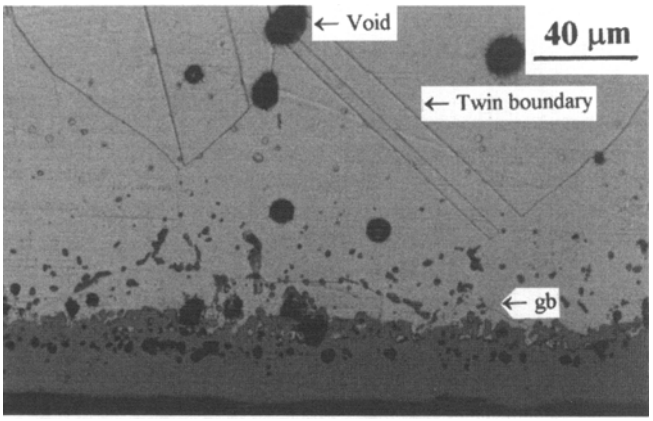


**Fig. 3** Optical micrograph showing matrix structure, internal oxidation, and voids formation along the grain and twin boundaries in the specimen exposed in steam (etched)

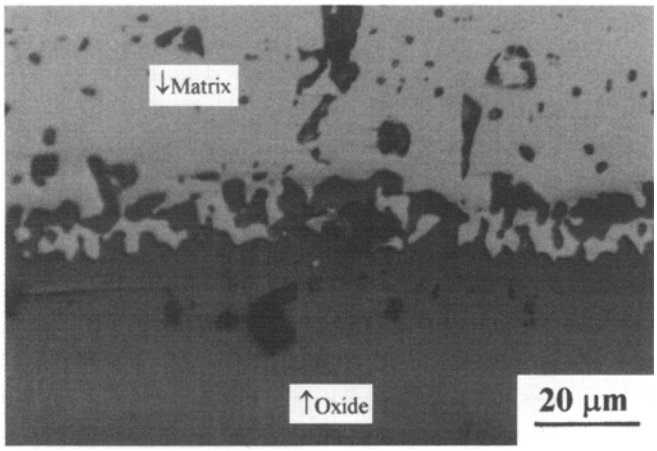


**Fig. 4** Optical micrograph showing oxide-metal interface structure (Nomanski interference contrast)

matrix is generally observed in the specimens exposed in air (for example, see Fig. 1b).

### 3.3 *Microanalysis of Oxidation*

Microanalysis of the matrix and oxide layer in the specimens is presented in Table 2. Trends are consistent with the oxidation kinetics reported elsewhere (Ref 7). The oxide layer can be seen to contain large amounts of Mn and Cr, indicating formation of $Cr_2O_3$ and complex spinels as described previously (Ref 5-7). Figure 6 shows an example of x-ray mapping across the oxide-metal interface that reveals a variation in the concentration of the elements during oxidation. Figure 7 shows certain concentration profiles of elements across different regions of metal and oxide where the variation in distribution of the elements in the matrix, voids, and internal and external oxide regions is evident. The amount of Cr and Mn increased in the external oxide layer, as compared to internal oxidation, and voids formed during oxidation. However, Ni and Mo concentration decreased in the internal and external oxide layers.

## 4. Conclusions

High-temperature oxidation behavior was studied in a nickel-base superalloy. The external oxide layer was dense and had a uniform thickness for the specimen exposed in steam, as compared to the cracking of the oxide and spallation observed in the specimen exposed in air. Evidence of voids in both the

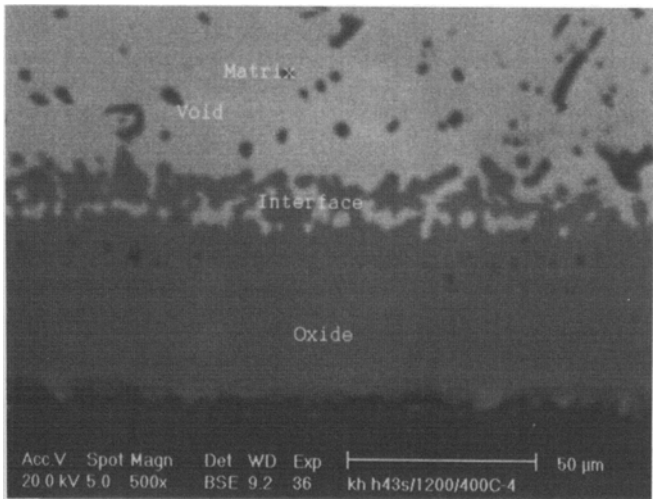


**Fig. 5** SEM backscattered micrograph showing dendritic interface between oxide and metal

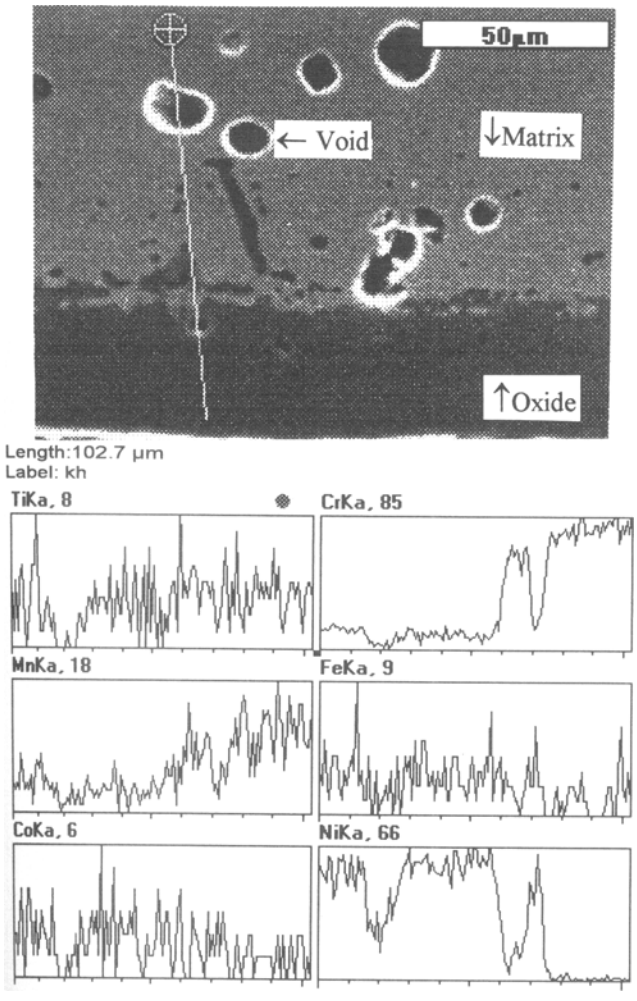


**Fig. 7** SEM linescan image and concentration profiles across voids (round), internal oxidation, and external oxide layer

matrix and the oxide layer was found. The network of internal oxidation was found along the grain and twin boundaries. The interface structure between oxide and metal revealed predominantly a dendritic growth morphology in the specimens exposed in steam as compared to the specimen exposed in air. Microanalysis showed a gradual increase in the concentration of Cr and Mn across the voids and internal and external oxide layers, whereas the amount of Ni and Mo decreased during oxidation. This effect was found to be enhanced in the case of the specimens exposed in steam as compared to the specimens exposed in air.

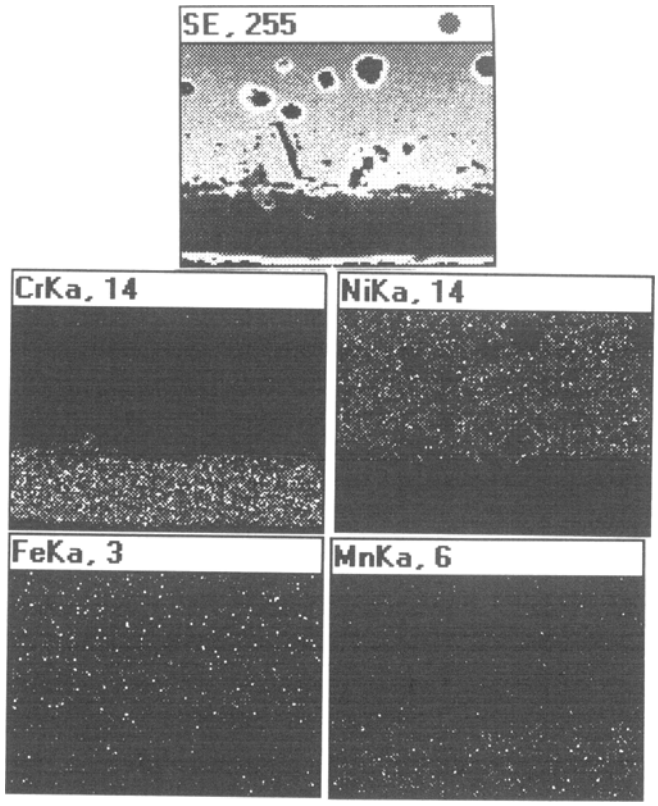


**Fig. 6** X-ray mapping across the oxide-metal interface

**Table 2 EDX microanalysis (fine spot) of matrix and external oxide layer**

| Exposure | Cr | Ni | Mn | Ti | Mo | Fe | Co |
|---|---|---|---|---|---|---|---|
| **Matrix** | | | | | | | |
| | 15.65 | 68.02 | 0.13 | 0.24 | 15.31 | 0.53 | 0.10 |
| **Oxide layer (specimens exposed in steam)** | | | | | | | |
| 1200 °C/6 h | 96.60 | 0.70 | 0.44 | 0.52 | 3.40 | ... | ... |
| 1000 °C/6 h | 81.80 | 13.00 | 1.60 | 1.0 | 1.50 | 0.70 | ... |
| **Oxide layer (specimens exposed in air)** | | | | | | | |
| 1200 °C/6 h | 34.70 | 2.80 | 0.34 | 1.15 | 5.20 | 0.16 | ... |
| 1000 °C/6 h | 23.00 | 61.00 | 1.42 | 0.73 | 7.00 | 0.25 | ... |

## Acknowledgments

GIK Institute is acknowledged for the provision of SEM laboratory facilities.

## References


1. T. Ericson, *Oxid. Met.*, Vol 2, 1970, p 401
2. T. Ishida, Y. Harayama, and S. Yaguchi, *J. Nucl. Mat.*, Vol 140, 1986, p 74
3. *Microscopy of Oxidation*, *Proc.*, Vol 2, S.B. Newcomb and M.J. Bennett, Ed., The Institute of Materials, 1993
4. P.H. Holloway, *J. Vac. Sci. Technol.*, Vol 18, 1981, p 653
5. D. Caplan and G.I. Sproule, *Oxid. Met.*, Vol 7, 1975, p 459
6. K.P. Lillerud and P. Kofstad, *J. Electrochem. Soc.*, Vol 127, 1980, p 2397
7. N. Hussain, K.A. Shahid, I.H. Khan, and S. Rahman, *Oxid. Met.*, Vol 41, 1994, p 253